# Effects of the on-site energy on the electronic response of $Sr_3(Ir_{1-x}Mn_x)_2O_7$

Dong Wook Kim<sup>1</sup>, G. Ahn<sup>1</sup>, J. Schmehr<sup>2</sup>, S. D. Wilson<sup>2</sup>, and S. J. Moon<sup>1,\*</sup>

<sup>1</sup>Department of Physics, Hanyang University, Seoul 04763, Republic of Korea

<sup>2</sup>Materials Department, University of California, Santa Barbara, CA 93106, USA

We investigated the doping and temperature evolutions of Sr<sub>3</sub>(Ir<sub>1-x</sub>Mn<sub>x</sub>)<sub>2</sub>O<sub>7</sub> single crystals with  $0 \le x \le 0.36$  by utilizing infrared spectroscopy. Mn substitution resulted in the development of a low-energy in-gap excitation at about 0.25 eV with the suppression of the optical excitations between the effective total angular momentum  $J_{\text{eff}}$  bands. The resonance energies of the optical transitions between the  $J_{\text{eff}}$  bands hardly varied with Mn substitution, suggesting the robustness of spin-orbit coupling effects. Mn substitution also led to the appearance of an optical excitation at about 1.2 eV, which is higher than the resonance energies of the optical transitions between the Jeff bands. The evolution of the electronic response with Mn substitution indicates that the Mn 3d states in Sr<sub>3</sub>(Ir<sub>1-x</sub>Mn<sub>x</sub>)<sub>2</sub>O<sub>7</sub> are located away from the Ir 5d states in energy, and the difference in the on-site energy is responsible for the incoherent charge transport and the resilience of the spinorbit coupling revealed in our optical data. The effect of Mn substitution was also registered in the temperature dependence of the electronic response. The anomaly in the optical response of the parent compound observed at the antiferromagnetic transition temperature is notably suppressed in the Mn-doped compounds despite the persistence of the long-range antiferromagnetic ordering. The suppression of the spin-charge coupling was attributed to charge disproportionation of the Ir ions

<sup>\*</sup>Correspondence and requests for materials should be addressed to S.J.M. (soonjmoon@hanyang.ac.kr)

# Introduction

Layered perovskite iridates of the  $Sr_{n+1}Ir_nO_{3n+1}$  (n = 1, 2) have attracted a great deal of attention as candidate systems from which unconventional superconductivity may emerge <sup>1-4</sup>.  $Sr_{n+1}Ir_nO_{3n+1}$  is an effective total angular momentum  $J_{eff} = 1/2$  Mott insulator realized by the cooperation of the moderate electronic correlations and strong spin-orbit coupling (SOC) <sup>5-7</sup>. The  $J_{eff} = 1/2$  Mott state of the iridates shares close similarities in its electromagnetic properties with the cuprates, which motivated intensive efforts to search for novel phases of the iridates by means of charge carrier doping. The representative cuprate phenomenology including the pseudogap <sup>8,9</sup>, the *d*-wave gap <sup>9,10</sup>, charge density wave <sup>11</sup> was also observed in doped iridates.

Since the Mott state of the iridates is stabilized by the strong SOC, it is expected that the reduction of the SOC may lead to an insulator-metal transition and associated novel phases. Theoretical studies suggested that the singlet d-wave and triplet p-wave pairing state could appear with the control of SOC [2,4]. The magnitude of the SOC is known to be proportional to the Z<sup>4</sup> (Z: atomic number) <sup>12</sup>, thus it can be controlled via substitution of Ir ions with other transition metal ions. A recent angle-resolved photoemission spectroscopy (ARPES) study on Sr<sub>2</sub>(Ir<sub>1-x</sub>Rh<sub>x</sub>)O<sub>4</sub> and Sr<sub>2</sub>(Ir<sub>1-x</sub>Ru<sub>x</sub>)O<sub>4</sub> suggested that the Rh/Ru doping resulted in the reduction of the SOC via hybridization between doped Rh/Ru ions and the host Ir ions, and this SOC reduction played a decisive role for their insulator-metal transition <sup>13</sup>. It was also suggested that the efficiency in the SOC dilution depended on the closeness of the on-site energies of the states of the Ir and Rh/Ru ions. On the other hand, another ARPES measurement indicated that the SOC did not control the insulator-metal transition of Sr<sub>2</sub>(Ir<sub>1-x</sub>Rh<sub>x</sub>)O<sub>4</sub> and Sr<sub>2</sub>(Ir<sub>1-x</sub>Ru<sub>x</sub>)O<sub>4</sub>. Instead, this study showed that the rigid band shift by hole doping and the appearance of the sets of bands with mostly Ru character generated by the hybridization between Ru and Ir ions drove the insulator-metal transition in  $Sr_2(Ir_{1-x}Rh_x)O_4$  and  $Sr_2(Ir_{1-x}Ru_x)O_4$ , respectively <sup>14</sup>. The difference of the origins of the insulator-metal transitions in the two systems were attributed to the difference in the on-site energies of the Rh and Ru ions.

Doping of 3d transition metal ions may be more effective in studying the effects of the change in the SOC to the electronic response of the iridates and the roles of the on-site energy of the host and impurity ions for the SOC dilution. Several studies investigated the transport and magnetic properties of Fe- or Co-doped Sr<sub>2</sub>IrO<sub>4</sub>, which showed that Fe or Co doping induced insulator-metal transitions. The insulator-metal transition was attributed to the formation of the impurity states close to the Fermi level. The effects of the Fe/Co doping on the electronic structure and the SOC, which can be gained by spectroscopy studies, were not

discussed in these reports  $^{15,16}$ . To the best of our knowledge, there is no optical spectroscopy reported on the 3d transition-metal-doped iridates.

In this paper, we studied the doping and temperature evolutions of the electronic response of Mn-doped Sr<sub>3</sub>Ir<sub>2</sub>O<sub>7</sub> single crystals, Sr<sub>3</sub>(Ir<sub>1-x</sub>Mn<sub>x</sub>)<sub>2</sub>O<sub>7</sub> with x = 0, 0.09, 0.18, 0.36 by means of infrared spectroscopy. The substitution of Mn ions,  $Mn^{3+}$  (3 $d^4$ ) or  $Mn^{4+}$  (3 $d^5$ ), is expected to dope holes to the system and to dilute the SOC, which can induce a insulator-metal transition. Upon Mn doping, the optical excitations between the J<sub>eff</sub> bands were suppressed and a lowenergy in-gap excitation at the energies  $\hbar\omega \leq 0.25$  eV appeared. The low-energy in-gap excitation reflects hole doping and is universally observed in doped iridates <sup>17-20</sup>. While the ingap excitation was enhanced with Mn doping, it did not evolve into the coherent Drude-like response in Sr<sub>3</sub>(Ir<sub>1-x</sub>Mn<sub>x</sub>)<sub>2</sub>O<sub>7</sub>, which is in sharp contrast to other doped iridates. In addition, the resonance energies of the optical excitations between the  $J_{\rm eff}$  bands hardly changes with Mn doping, indicating the stiffness of the SOC. At  $\hbar\omega \geq 1$  eV, a distinct optical excitation which has not been observed in 4d transition-metal doped iridates, such as Sr<sub>2</sub>(Ir,Rh)O<sub>4</sub> and Sr<sub>n+1</sub>(Ir,Ru)<sub>n</sub>O<sub>3n+1</sub>, emerged with Mn doping. The resonance energy of this optical excitation is higher than those of the transitions between  $J_{\text{eff}}$  bands. The observation of the high-energy optical transition suggests that the on-site energy of Mn ions is quite different from that of Ir ions. The large difference in the on-site energies can lead to a strong disorder and a resilience of the SOC and thus can be associated with the absence of the insulator-metal transition in  $Sr_3(Ir_{1-x}Mn_x)_2O_7$ . Mn doping also alters the temperature evolution of the electronic response. The strong anomaly in the optical response of the parent compound at the antiferromagnetic transition temperature T<sub>N</sub> disappeared upon Mn doping, which we attributed to charge disproportionation of the Ir ions.

## Results and discussion

**Doping evolution of the optical response.** Figure 1 shows the real part of the optical conductivity spectra  $\sigma_1(\omega)$  of Sr<sub>3</sub>(Ir<sub>1-x</sub>Mn<sub>x</sub>)<sub>2</sub>O<sub>7</sub>. In the  $\sigma_1(\omega)$  of the parent compound, two prominent peaks, labeled as  $\alpha$  and  $\beta$  are observed. The peak  $\alpha$  corresponds to the optical transition from the  $J_{\text{eff}} = 1/2$  lower Hubbard band (LHB) to the  $J_{\text{eff}} = 1/2$  upper Hubbard band (UHB). The peak  $\beta$  corresponds to the optical transitions from the  $J_{\text{eff}} = 3/2$  bands to the  $J_{\text{eff}} = 1/2$  UHB stransition is composed of two peaks, i.e.,  $\beta$  and  $\gamma$ , as shown in Fig. 1(e). Upon Mn doping, the peaks  $\alpha$  and  $\beta$  are suppressed and an

in-gap excitation labeled as A appears below about 0.25 eV. In addition to the change in the lowenergy response, Mn doping induces an enhancement of  $\sigma_1(\omega)$  in the energy region between 1 and 2 eV, where in the parent compound the peak  $\gamma$ , the optical transition from the  $J_{\text{eff}} = 3/2$ bands to the  $J_{\text{eff}} = 1/2$  upper Hubbard band, is located. Since the peak  $\gamma$  should be suppressed in the Mn-doped samples, similar to the peaks  $\alpha$  and  $\beta$ , the majority of the spectral weight in the energy region between 1 and 2 eV for the Mn-doped compound could not be attributed to the optical transition between the  $J_{\text{eff}}$  bands but should be attributed with transition associated with the Mn states. To reflect its distinct nature, we labeled the peak at about 1.2 eV in the Mn-doped samples as C.

Optical conductivity data at 10 K in Fig. 2(a) illustrate the evolution of the electronic structure with Mn doping more clearly. One of the most prominent changes is the drastic suppression of the peak  $\alpha$ . Part of the spectral weight of the peak  $\alpha$  is shifted across an isosbestic point at about 0.25 eV to the lower-energy in-gap excitation, peak A, which is one of the universal characteristic features of the filling-controlled insulator-metal transition in correlated electron systems <sup>22,23</sup>. For a system exhibiting the filling-controlled insulator-metal transition, charge carrier doping leads to a suppression of the optical transitions across the gap and spectral weight shift to fill the gap with an incoherent in-gap excitations. Upon further doping, a weak coherent Drude-like response appears before a fully coherent Drude-like peak develops with the merger between the coherent and the incoherent responses. These universal behaviors were registered in the optical response of Rh- or Ru-doped  $Sr_{n+1}Ir_nO_{3n+1}$  (n=1,2). Both the Rh and Ru substitution result in holedoping and induces a insulator-metal transition. In the optical conductivity data of Sr<sub>2</sub>(Ir,Rh)O<sub>4</sub> and Sr<sub>3</sub>(Ir,Ru)<sub>2</sub>O<sub>7</sub>, a clear Drude-like peak appeared upon 5% Rh and 34% Ru doping, respectively <sup>17,19</sup>. In sharp contrast, for Sr<sub>3</sub>(Ir<sub>1</sub>- $_xMn_x)_2O_7$ , the incoherent in-gap excitation does not evolve into the coherent Drude-like peak but remains incoherent up to the highest Mn concentration of x = 0.36, which suggests that the doped holes remain localized.

Anderson localization can be responsible for the incoherent nature of the low-energy optical response  $^{24,25}$ . Anderson localization is mainly due to disorders in the system. In a correlated Mott system, the cooperation between the randomness and the electronic correlations can induce a soft gap in the electronic density of states  $^{25-29}$ , thus hindering coherent charge transport. Accordingly, the dc resistivity follows variable-range hopping (VRH)  $^{30}$ . The resistivity data of Sr<sub>3</sub>(Ir<sub>1-x</sub>Mn<sub>x</sub>)<sub>2</sub>O<sub>7</sub> indeed display the VRH behavior in a wide range of

temperature <sup>31</sup>. We note that the VRH behavior of the dc resistivity was also registered in insulating/bad metallic Rh- and Tb-doped Sr<sub>2</sub>IrO<sub>4</sub> compounds <sup>32,33</sup>.

In order to obtain more quantitative information on the evolution of the electronic structure with Mn doping, we analyzed the  $\sigma_1(\omega)$  using Lorentz oscillator model:

$$\sigma_1(\omega) = \sum_k \frac{S_k^2}{4\pi} \frac{\omega^2 \gamma_k}{(\omega^2 - \omega_{0k}^2)^2 + \omega^2 \gamma_k},\tag{1}$$

where  $S_k$  is the strength and  $\omega_{0,k}$ ,  $\gamma_k$  are the resonant frequency, the width of the Lorentz oscillator, respectively. The result of the Lorentz oscillator model fit for the 10 K data of  $Sr_3(Ir_1 xMn_x)_2O_7$  is displayed in Figs. 1(e)-1(h). Three  $(\alpha, \beta, \gamma)$  and five  $(\alpha, \beta, A, B, C)$  Lorentz oscillators are needed to reproduce the  $\sigma_1(\omega)$  data of the parent and Mn-doped compounds, respectively. The peak A represents the in-gap excitation. The peak B is required to account for the little change in  $\sigma_1(\omega)$  at about 0.6 - 0.7 eV despite the suppression of the peak  $\beta$ . The parameters extracted from the fitting are summarized in Figs. 2(b) and 2(c).

The Lorentz oscillator model analysis provides important information on the evolution of the electronic structure of  $Sr_3(Ir_{1-x}Mn_x)_2O_7$ . We note that the resonance energies of the peak  $\alpha$  and  $\beta$  hardly change with Mn doping, as shown in Fig. 2(b). It should be mentioned that, whereas the resonance energy of the peak  $\beta$  is not clearly resolved in  $\sigma_1(\omega)$  due to its overlap with the neighboring optical transitions, it can be identified in the imaginary part of the dielectric function  $\varepsilon_2(\omega)$  [inset of Fig. 2(a)]. Since the separation of the peaks  $\alpha$  and  $\beta$  is proportional to the magnitude of the SOC,  $\lambda_{SO}$ , this observation indicates that the SOC is resilient against Mn doping. The robustness of the SOC in the Mn-doped compounds samples is further supported by the large branching ratio from a recent x-ray absorption spectroscopy study  $^{31}$ .

A recent ARPES study on Sr<sub>2</sub>(Ir,Ru)O<sub>4</sub> and Sr<sub>2</sub>(Ir,Rh)O<sub>4</sub> suggested that the reduction of the SOC is strongly dependent on the impurity potential <sup>13</sup>. It was shown that the large difference between the on-site energies of the host (Ir) and impurity (Ru/Rh) states can prevent their hybridization and thus the dilution of the SOC. Our observation of the robustness of the SOC as well as the incoherent charge transport of Sr<sub>3</sub>(Ir<sub>1-x</sub>Mn<sub>x</sub>)<sub>2</sub>O<sub>7</sub> suggests that the Mn states may be located away from the Ir states in energy.

The strong enhancement of  $\sigma_1(\omega)$  in the energy region between 1 and 1.5 eV, which leads

to the development of the peak C, with Mn doping indicates that the Mn states are indeed located away from the Ir  $J_{\rm eff} = 1/2$  states in energy: the resonance energy of the peak C is larger than those of the optical transitions between the  $J_{\rm eff} = 1/2$  bands. In Sr<sub>3</sub>(Ir,Ru)<sub>2</sub>O<sub>7</sub> and Sr<sub>2</sub>(Ir,Rh)O<sub>4</sub> where the Ru or Rh states were closer in energy to the Ir  $J_{\rm eff} = 1/2$  bands<sup>13,14</sup> than the Mn states, Ru or Rh substitution do not induce the enhancement of  $\sigma_1(\omega)$  in the energy region between 1 and 1.5 eV <sup>17-19,34</sup>, as shown in Figs. 3(a) and 3(b).

The assignment of the peak C should depend on the valence state of Mn ions  $^{35\text{-}37}$ . In perovskite manganites, Mn ions can have  $4+(3d^3)$  or  $3+(3d^4)$  valence state. For Mn<sup>4+</sup> ions, the doubly-degenerate  $e_g$  spin-up  $(e_g^{\uparrow})$  bands are closest to the Fermi level: it is located above the Fermi level by about 1.71 eV in Sr<sub>3</sub>Mn<sub>2</sub>O<sub>7</sub>  $^{38}$ . For Mn<sup>3+</sup> ions, the degeneracy of the  $e_g^{\uparrow}$  bands is lifted by Jahn-Teller effects and the split  $e_{g,1}^{\uparrow}$  and  $e_{g,2}^{\uparrow}$  bands are located above and below the Fermi level by at least about 0.6 eV  $^{39}$ .

Magnetization measurements of Sr<sub>3</sub>(Ir<sub>1-x</sub>Mn<sub>x</sub>)<sub>2</sub>O<sub>7</sub> suggested a shift in the Mn valence from 4+ to 3+ at  $x \approx 0.25^{-31}$ . However, a comparison between the low-energy optical response of  $Sr_3(Ir_{1-x}Mn_x)_2O_7$  and  $Sr_3(Ir,Ru)_2O_7/Sr_2(Ir,Rh)O_4$  suggests that  $Mn^{3+}$  ions should exist in x=0.09and 0.18 samples. As shown in Fig. 3(a), the conductivity data of Sr<sub>3</sub>(Ir,Ru)<sub>2</sub>O<sub>7</sub> barely changes even upon 22% Ru doping <sup>19</sup>. The peak  $\alpha$  is remains robust against Ru doping and in-gap excitations do not emerge. The sizeable changes in  $\sigma_1(\omega)$  occur only beyond the critical Ru concentration of about 0.35 at which the transport data indicates a insulator-to-metal transition <sup>40</sup>. This behavior suggests that the charge transfer between Ir<sup>4+</sup> and Ru<sup>4+</sup> ions are prohibited, thus protecting 4+ valence of Ir ions <sup>40-42</sup>. In contrast, it is known that Rh substitution induces hole-doping on the Ir sites via electron transfer from Ir ions to Rh at low Rh concentrations, introducing Ir<sup>5+</sup> and Rh<sup>3+</sup> pairs <sup>43-46</sup>. The corresponding  $\sigma_1(\omega)$  of Sr<sub>2</sub>(Ir,Rh)O<sub>4</sub> exhibits the suppression of the peak  $\alpha$  and the emergence of an in-gap excitation <sup>17</sup>. The close similarities between the optical responses of Sr<sub>3</sub>(Ir<sub>1-x</sub>Mn<sub>x</sub>)<sub>2</sub>O<sub>7</sub> and Sr<sub>2</sub>(Ir,Rh)O<sub>4</sub> suggest that Mn substitution changes the filling of the  $J_{\rm eff} = 1/2$  LHB via hole-doping and induces the formation of Mn<sup>3+</sup> and Ir<sup>5+</sup> ions. Therefore, we suggest that Mn<sup>3+</sup> ions coexist with majority Mn<sup>4+</sup> ions at low Mn concentrations and the portion of Mn<sup>3+</sup> ions increases with increasing Mn doping. Based on the inference of the valence of Mn ions from the magnetization measurements 31 and our optical data, the peak C can be assigned mainly as a transition from  $J_{\text{eff}} = 3/2$  state to Mn  $e_q^{\uparrow}$  state for x = 0.09 and 0.18 and a transition from  $J_{\text{eff}} = 3/2$  to Mn  $e_{g,2}^{\uparrow}$  state for x = 0.36 compound. Then,

the peak B at about 0.68 eV can be assigned as a transition from  $J_{\text{eff}} = 1/2$  LHB to Mn  $e_g^{\uparrow}$  state. The corresponding schematic diagrams of the electronic density of states are displayed in Figs. 2(d) and 2(e).

The variation of the SW of the peak B and C with Mn doping supports the assignments. As shown in Fig. 2(c), the peak C is enhanced with Mn doping up to x = 0.18 but is suppressed with further Mn doping. The peak B also exhibits a rapid enhancement as x changes from 0.18 to 0.36. When the valence of Mn ions changes from 4+ and 3+, the Mn  $e_g^{\uparrow}$  state can split into  $e_{g,1}^{\uparrow}$  and  $e_{g,2}^{\uparrow}$  due to the Jahn-Teller effect, resulting in the decrease of the density of states of the  $e_g^{\uparrow}$  state. Therefore, the SW of the peak C, a transition from the  $J_{\rm eff} = 3/2$  state to Mn  $e_g^{\uparrow}$  state should be suppressed. In order to account for the enhancement of the peak B, the split  $e_{g,1}^{\uparrow}$  state should be located between the  $J_{\rm eff} = 3/2$  and the  $J_{\rm eff} = 1/2$  LHB, so that an optical transition from the Mn  $e_{g,1}^{\uparrow}$  state to the  $J_{\rm eff} = 1/2$  UHB contributes to the spectral weight at the energies where the peak B is located. Further studies are desired to investigate the effects of the Jahn-Teller splitting of Mn  $e_g^{\uparrow}$  states.

Temperature evolution of the optical response. Having identified the effects of Mn doping to the ground-state electronic structure, we discuss the temperature evolution of the low-energy optical response. In the parent compound, the optical conductivity data show clear anomalies at the antiferromagnetic transition temperature  $T_N$ , implying a strong spin-charge coupling <sup>18</sup>. As the temperature increases across  $T_N$ , the peak  $\alpha$  exhibits an abrupt redshift <sup>18</sup>. In addition, the the in-gap spectral weight obtained by the integration of  $\sigma_1(\omega)$  up to the isosbestic point of  $\omega_0 = 0.35$  eV,  $SW(\omega_c) = \int_0^{\omega_c} \sigma_1(\omega) d\omega$  is significantly enhanced at  $T_N$  [Fig. 4(e)]. A combined optical spectroscopy and ARPES study demonstrated that these changes in  $\sigma_1(\omega)$  were attributed to a magnetically driven band shift toward the Fermi level with the suppression of the antiferromagnetic order <sup>18</sup>.

The temperature evolutions of the low-energy optical responses of the Mn-doped compounds suggest that Mn-doping suppresses the spin-charge coupling. Figures 4(b)-4(d) show that the resonance energy of the peak  $\alpha$ , which corresponds to the distance between the  $J_{\text{eff}} = 1/2$  LHB and UHB, is independent of temperature. This observation indicates that the shift of the  $J_{\text{eff}} = 1/2$  Hubbard bands in energy due to the antiferromagnetic order does not occur in the Mn-doped compounds. In addition, the in-gap spectral weights SW( $\alpha$ c) of Sr<sub>3</sub>(Ir<sub>1</sub>-

 $_x$ Mn $_x$ )<sub>2</sub>O<sub>7</sub> calculated with  $\omega_c$  = 0.34 (x = 0.09), 0.36 (x = 0.18), 0.33 eV (x = 0.36) show gradual changes with the variation in temperature without showing any anomaly. In addition to the absence of the anomaly at  $T_N$ , the magnitude of the change in the SW decreases with Mn doping. It is worth pointing out that the long-range antiferromagnetic order of the  $J_{eff}$  = 1/2 pseudospin survives up to x = 0.25  $^{31}$ .

The temperature dependence of the optical response of  $Sr_3(Ir_{1-x}Mn_x)_2O_7$  should be contrasted to that of  $Sr_3(Ir,Ru)_2O_7$ . In the latter system, the anomaly in  $\sigma_1(\omega)$  at  $T_N$ , related to the redshift of the peak  $\alpha$  and the increase in the  $SW(\omega_c)$  observed in the parent compound, remained robust up to the Ru concentration of 0.34, above which the long-range antiferromagnetic order disappeared <sup>18,19</sup>. The clear distinction between the Mn- and Ru-doped compounds may be attributed to the different valence states of the dopant ions. Since Ru ion (4+) is isovalent with Ir ions in  $Sr_3(Ir,Ru)_2O_7$ , the holes tend to be localized at the Ru sites <sup>40</sup>. Therefore, the  $J_{eff}=1/2$  pseudospin can remain intact despite a substantial Ru doping. Conversely, as inferred from our optical data, Mn doping induces formation of  $Ir^{5+}$  ions. Thus, the Ir ions near the doped Mn ions can lose their  $J_{eff}=1/2$  pseudospin. We conjecture that this charge disproportionation and the resulting loss of the pseudospin may be responsible for the suppression of the spin-charge coupling in  $Sr_3(Ir_{1-x}Mn_x)_2O_7$ .

#### **Conclusion**

We studied the doping and temperature dependence of the optical response of  $Sr_3(Ir_{1-x}Mn_x)_2O_7$  with  $0 \le x \le 0.36$ . We observed that the Mn substitution resulted in the suppression of the Mott gap excitation and the appearance of an in-gap excitation, which is one of the characteristic features of charge carrier doping. The in-gap excitation did not evolve into the Drude-like peak, but remained incoherent up to highest Mn concentration possibly due to the Anderson localization. While the optical excitations between the Ir  $J_{eff}$  bands were suppressed, their resonance energies did not change, indicating the robustness of the SOC. Mn doping induced an enhancement of the optical conductivity for energies above 1 eV, which indicates that the on-site energy of the Mn states is quite different from that of the Ir  $J_{eff} = 1/2$  bands. The doping evolution of the optical response suggests that the Anderson localization and the robustness of the SOC are likely to be attributed to the large difference between the on-site energies of the Mn and Ir states. The temperature dependence of the electronic response was significantly affected by Mn doping. The anomalies of the optical response at the antiferromagnetic ordering

temperature, the energy shift of the optical transition between the  $J_{\rm eff} = 1/2$  Hubbard bands and

the abrupt change in the SW of the in-gap excitation observed in the parent compound,

disappeared in the Mn-doped compounds. We ascribe this phenomenon of the spin-charge

decoupling to the charge disproportionation due to Mn substitution, resulting in the loss of  $J_{\text{eff}}$ 

= 1/2 pseudospin.

Methods

High-quality single crystals of  $Sr_3(Ir_{1-x}Mn_x)_2O_7$  with x = 0, 0.09, 0.18, 0.36 were grown using

a halide flux growth technique. Details of the single crystal growth were described in Ref. <sup>31</sup>.

We measured near-normal incidence reflectivity spectra  $R(\omega)$  in the energy region between 5

meV and 1 eV using Fourier transform infrared spectrometer (Vertex 70v, Bruker). We

employed *in-situ* gold overcoating technique to obtain accurate reflectivity data <sup>47</sup>. Complex

optical constants in the energy region between 0.74 and 5 eV were obtained using spectroscopic

ellipsometer (M-2000, J. A. Woollam Co.). Optical conductivity was calculated from the  $R(\omega)$ 

data through Kramers-Kronig transformation.

Acknowledgements

This research was supported by the National Research Foundation grant of Korea (NRF) funded

by the Korean government (MSIT) (2022R1F1A1072865) and BrainLink program funded by

the Ministry of Science and ICT through the National Research Foundation of Korea

(2022H1D3A3A01077468). S.D.W. and J.S. acknowledge support from National Science

Foundation award DMR-1905801.

**Author Contributions** 

D.W.K. and S.J.M. conceived the project. D.W.K. carried out the optical measurements. D.W.K.,

G.A., and S.J.M. analyzed the optical data. J. S and S.D.W grew and characterized the single

crystals. All authors participated in discussing the results and writing the manuscript.

**Competing financial interest:** The authors declare no competing financial interest.

9

# **Figure Captions**

**Figure 1.** Temperature dependent optical conductivity spectra  $\sigma(\omega)$  of Sr<sub>3</sub>(Ir<sub>1-x</sub>Mn<sub>x</sub>)<sub>2</sub>O<sub>7</sub> for (a) x = 0, (b) x = 0.09, (c) x = 0.18, (d) x = 0.36 from T = 10 K to 300 K. Fitting results of Lorentz oscillator model for (e) x = 0, (f) x = 0.09, (g) x = 0.18, (h) x = 0.36 at T = 10 K.

**Figure 2.** (a) Optical conductivity spectra of  $Sr_3(Ir_{1-x}Mn_x)_2O_7$  at 10 K. The inset shows the imaginary parts of the dielectric constant. (b) Doping dependence of the resonance energies of the peaks  $\alpha$ ,  $\beta$ , A, B,  $C(\gamma)$  at 10 K. (c) Doping dependence of the spectral weights of the peaks  $\alpha$ ,  $\beta$ , A, B,  $C(\gamma)$ . The inset shows the doping dependence of the SW of the peak C. Schematic band diagram of  $Sr_3(Ir_{1-x}Mn_x)_2O_7$  with the cases where (d) the  $Mn^{4+}$  and (e)  $Mn^{3+}$  ions dominate. The bands drawn with dashed lines in (d) represent the  $e_{g,1}^{\uparrow}$  and  $e_{g,2}^{\uparrow}$  states of the minority  $Mn^{3+}$  ions in the x = 0.09 and 0.18 compounds.

**Figure 3.** Optical conductivity spectra of (a)  $Sr_3Ir_2O_7$ ,  $Sr_3(Ir_{0.78}Ru_{0.22})_2O_7$ ,  $Sr_3(Ir_{0.64}Mn_{0.36})_2O_7$  and (b)  $Sr_2IrO_4$ ,  $Sr_2Ir_{0.96}Rh_{0.04}O_4$ .

**Figure 4.** Temperature dependence of the peak  $\alpha$  of Sr<sub>3</sub>(Ir<sub>1-x</sub>Mn<sub>x</sub>)<sub>2</sub>O<sub>7</sub> with (a) x = 0, (b) x = 0.09, (c) x = 0.18, (d) x = 0.36. Temperature dependence of the optical SW( $\omega_c$ ) for (f) x = 0 ( $\omega_c = 0.34$  eV), (g) x = 0.09 ( $\omega_c = 0.34$  eV), (h) x = 0.18 ( $\omega_c = 0.36$  eV) and (i) x = 0.36 ( $\omega_c = 0.33$ eV). The dashed lines in (f)-(i) denote the Néel temperature for each sample.

## References

- Wang, F. & Senthil, T. Twisted Hubbard Model for Sr<sub>2</sub>IrO<sub>4</sub>: Magnetism and Possible High Temperature Superconductivity. *Phys. Rev. Lett.* **106**, 136402 (2011).
- Meng, Z. Y., Kim, Y. B. & Kee, H. Y. Odd-Parity Triplet Superconducting Phase in Multiorbital Materials with a Strong Spin-Orbit Coupling: Application to Doped Sr<sub>2</sub>IrO<sub>4</sub>. *Phys. Rev. Lett.* **113**, 177003 (2014).
- Sumita, S., Nomoto, T. & Yanase, Y. Multipole Superconductivity in Nonsymmorphic Sr<sub>2</sub>IrO<sub>4</sub>. *Phys. Rev. Lett.* **119**, 027001 (2017).
- Watanabe, H., Shirakawa, T. & Yunoki, S. Monte Carlo study of an unconventional superconducting phase in iridium oxide  $J_{\text{eff}} = 1/2$  Mott insulators induced by carrier doping. *Phys. Rev. Lett.* **110**, 027002 (2013).
- Kim, B. J. *et al.* Novel  $J_{\text{eff}} = 1/2$  Mott state induced by relativistic spin-orbit coupling in Sr<sub>2</sub>IrO<sub>4</sub>. *Phys. Rev. Lett.* **101**, 076402 (2008).
- 6 Kim, B. J. *et al.* Phase-Sensitive Observation of a Spin-Orbital Mott State in in Sr<sub>2</sub>IrO<sub>4</sub>. *Science* **323**, 1329-1332 (2009).
- Moon, S. J. *et al.* Dimensionality-controlled insulator-metal transition and correlated metallic state in 5*d* transition metal oxides  $Sr_{n+1}Ir_nO_{3n+1}$  (n = 1, 2, and  $\infty$ ). *Phys. Rev. Lett.* **101**, 226402 (2008).
- 8 Kim, Y. K. *et al.* Superconductivity. Fermi arcs in a doped pseudospin-1/2 Heisenberg antiferromagnet. *Science* **345**, 187-190 (2014).
- 9 Yan, Y. J. *et al.* Electron-Doped Sr<sub>2</sub>IrO<sub>4</sub>: An Analogue of Hole-Doped Cuprate Superconductors Demonstrated by Scanning Tunneling Microscopy. *Phys. Rev. X* 5, 041018 (2015).
- Kim, Y. K., Sung, N. H., Denlinger, J. D. & Kim, B. J. Observation of a *d*-wave gap in electron-doped Sr<sub>2</sub>IrO<sub>4</sub>. *Nat. Phys.* **12**, 37-41 (2015).
- 11 Chu, H. *et al.* A charge density wave-like instability in a doped spin-orbit-assisted weak Mott insulator. *Nat Mater* **16**, 200-203 (2017).
- Shanavas, K. V., Popović, Z. S. & Satpathy, S. Theoretical model for Rashba spin-orbit interaction in *d* electrons. *Phys. Rev. B* **90**, 165108 (2014).
- Zwartsenberg, B. *et al.* Spin-orbit-controlled metal-insulator transition in Sr<sub>2</sub>IrO<sub>4</sub>. *Nat. Phys.* **16**, 290-294 (2020).
- Brouet, V. *et al.* Origin of the different electronic structure of Rh- and Ru-doped Sr<sub>2</sub>IrO<sub>4</sub>. *Phys. Rev. B* **104**, L121104 (2021).
- Hu, B. *et al.* Correlation between antiferromagnetic and Mott states in spin orbit coupled Sr<sub>2</sub>IrO<sub>4</sub>: A study of Sr<sub>2</sub>Ir $_{-x}$ M $_x$ O<sub>4</sub> (M = Fe or Co). *Phys. Rev. B* **103**, 115122 (2021).
- Samanta, K. et al. Quantum criticality in a layered iridate. Commun. Phys. 4, 89 (2021).
- 17 Xu, B. *et al.* Optical Signature of a Crossover from Mott- to Slater-Type Gap in Sr<sub>2</sub>Ir<sub>1-x</sub>Rh<sub>x</sub>O<sub>4</sub>. *Phys. Rev. Lett.* **124**, 027402 (2020).
- Song, S. *et al.* Magnetically driven band shift and metal-insulator transition in spin-orbit-coupled Sr<sub>3</sub>(Ir<sub>1-x</sub>Ru<sub>x</sub>)<sub>2</sub>O<sub>7</sub>. *Phys. Rev. B* **98**, 035110 (2018).
- Ahn, G., Schmehr, J. L., Porter, Z., Wilson, S. D. & Moon, S. J. Doping and temperature evolutions of optical response of Sr<sub>3</sub>(Ir<sub>1-x</sub>Ru<sub>x</sub>)<sub>2</sub>O<sub>7</sub>. *Sci Rep* **10**, 22340 (2020).
- Lee, S. *et al.* Evolution of the electronic structure of Ru-doped single-crystal iridates Sr<sub>2</sub>Ir<sub>1-x</sub>Ru<sub>x</sub>O<sub>4</sub>. *Phys. Rev. B* **104**, 165106 (2021).
- Moon, S. J. et al. Temperature dependence of the electronic structure of the  $J_{\text{eff}} = 1/2$  Mott

- insulator Sr<sub>2</sub>IrO<sub>4</sub> studied by optical spectroscopy. Phys. Rev. B 80, 195110 (2009).
- Basov, D. N., Averitt, R. D., van der Marel, D., Dressel, M. & Haule, K. Electrodynamics of correlated electron materials. *Rev. Mod. Phys.* **83**, 471-541 (2011).
- Imada, M., Fujimori, A. & Tokura, Y. Metal-insulator transitions. *Rev. Mod. Phys.* **70**, 1039-1263 (1998).
- Anderson, P. W. Absence of Diffusion in Certain Random Lattices. *Phys. Rev.* **109**, 1492-1505 (1958).
- Shinaoka, H. & Imada, M. Theory of Electron Transport near Anderson–Mott Transitions. *J. Phys. Soc. Jpn.* **79**, 113703 (2010).
- Chiesa, S., Chakraborty, P. B., Pickett, W. E. & Scalettar, R. T. Disorder-induced stabilization of the pseudogap in strongly correlated systems. *Phys. Rev. Lett.* **101**, 086401 (2008).
- Fazileh, F., Gooding, R. J., Atkinson, W. A. & Johnston, D. C. Role of Strong Electronic Correlations in the Metal-To-Insulator Transition in Disordered LiAlyTi<sub>2-y</sub>O<sub>4</sub>. *Phys. Rev. Lett.* **96**, 046410 (2006).
- Byczuk, K., Hofstetter, W. & Vollhardt, D. Mott-Hubbard transition versus Anderson localization in correlated electron systems with disorder. *Phys. Rev. Lett.* **94**, 056404 (2005).
- Shinaoka, H. & Imada, M. Single-Particle Excitations under Coexisting Electron Correlation and Disorder: A Numerical Study of the Anderson–Hubbard Model. *J. Phys. Soc. Jpn.* **78**, 094708 (2009).
- Efros, A. L. & Shklovskii, B. I. Coulomb gap and low temperature conductivity of disordered systems. *J. Phys. C: Solid State Phys.* **8**, L49-L51 (1975).
- 31 Schmehr, J. L. *et al.* Preferential quenching of 5d antiferromagnetic order in  $Sr_3(Ir_{1-x}Mn_x)$  207. *J. Phys. Condens. Matter* **31**, 244003 (2019).
- Qi, T. F. *et al.* Spin-orbit tuned metal-insulator transitions in single-crystal  $Sr_2Ir_{1-x}Rh_xO_4$  ( $0 \le x \le 1$ ). *Phys. Rev. B* **86**, 125105 (2012).
- Wang, J. C. *et al.* Decoupling of the antiferromagnetic and insulating states in Tb-doped Sr<sub>2</sub>IrO<sub>4</sub>. *Phys. Rev. B* **92**, 214411 (2015).
- Lee, J. S., Krockenberger, Y., Takahashi, K. S., Kawasaki, M. & Tokura, Y. Insulator-metal transition driven by change of doping and spin-orbit interaction in Sr<sub>2</sub>IrO<sub>4</sub>. *Phys. Rev. B* **85**, 035101 (2012).
- Jung, J. H. *et al.* Determination of electronic band structures of CaMnO<sub>3</sub> and LaMnO<sub>3</sub> using optical-conductivity analyses. *Phys. Rev. B* **55**, 15489-15493 (1997).
- Lee, Y. et al. Correlation of electronic structure and ordered charge and orbital patterns for single-layered manganites in a wide hole-doping range  $(0 \le x \le 1)$ . Phys. Rev. B 75, 144407 (2007).
- Ishikawa, T., Tobe, K., Kimura, T., Katsufuji, T. & Tokura, Y. Optical study on the doping and temperature dependence of the anisotropic electronic structure in bilayered manganites: La<sub>2-2x</sub>Sr<sub>1+2x</sub>Mn<sub>2</sub>O<sub>7</sub> (0.3<-x<-0.5). *Phys. Rev. B* **62**, 12354-12362 (2000).
- Meskine, H., Popović, Z. S. & Satpathy, S. Electronic structure and exchange interaction in the layered perovskite Sr<sub>3</sub>Mn<sub>2</sub>O<sub>7</sub>. *Phys. Rev. B* **65**, 094402 (2002).
- Park, K. T. Electronic structure calculations for layered LaSrMnO<sub>4</sub> and Ca<sub>2</sub>RuO<sub>4</sub>. *J. Condens. Matter Phys.* **13**, 9231 (2001).
- Dhital, C. *et al.* Carrier localization and electronic phase separation in a doped spin-orbit-driven Mott phase in Sr<sub>3</sub>(Ir<sub>1-x</sub>Ru<sub>x</sub>)<sub>2</sub>O<sub>7</sub>. *Nat. Commun.* 5, 1-7 (2014).
- Schmehr, J. L. *et al.* Overdamped Antiferromagnetic Strange Metal State in Sr<sub>3</sub>IrRuO<sub>7</sub>. *Phys. Rev. Lett.* **122**, 157201 (2019).

- Cava, R. J. *et al.* Localized-to-itinerant electron transition in Sr<sub>2</sub>Ir<sub>1-x</sub>Ru<sub>x</sub>O<sub>4</sub>. *Phys. Rev. B* **49**, 11890-11894 (1994).
- Cao, Y. *et al.* Hallmarks of the Mott-metal crossover in the hole-doped pseudospin-1/2 Mott insulator Sr<sub>2</sub>IrO<sub>4</sub>. *Nat. Commun.* 7, 11367 (2016).
- Chikara, S. *et al.* Charge partitioning and anomalous hole doping in Rh-doped Sr<sub>2</sub>IrO<sub>4</sub>. *Phys. Rev. Lett.* **95**, 060407 (2017).
- Clancy, J. P. *et al.* Dilute magnetism and spin-orbital percolation effects in Sr<sub>2</sub>Ir<sub>1-x</sub>Rh<sub>x</sub>O<sub>4</sub>. *Phys. Rev. B* **89**, 054409 (2014).
- Louat, A. *et al.* Formation of an incoherent metallic state in Rh-doped Sr<sub>2</sub>IrO<sub>4</sub>. *Phys. Rev. B* **97**, 161109 (2018).
- Homes, C. C., Reedyk, M., Cradles, D. A. & Timusk, T. Technique for measuring the reflectance of irregular, submillimeter-sized samples. *Appl. Opt.* **32**, 2976-2983 (1993).

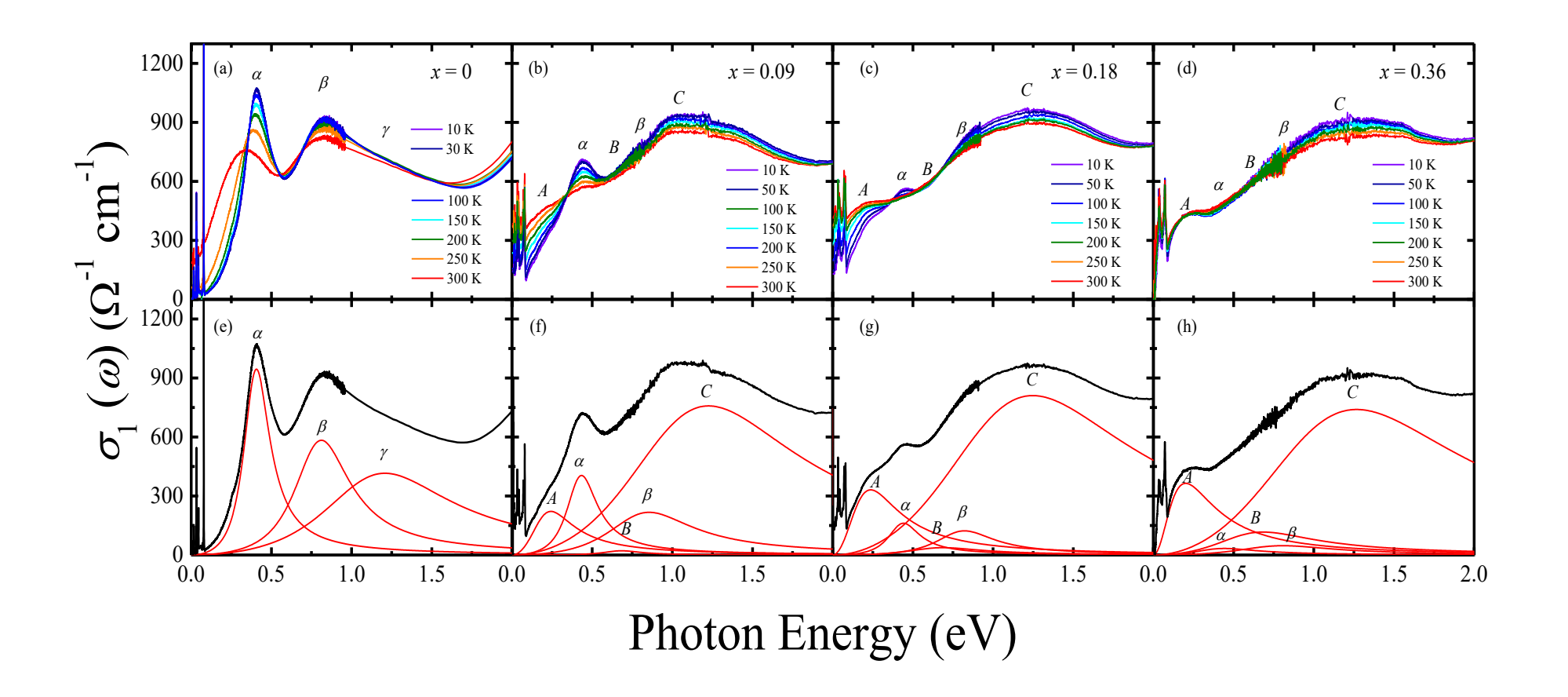


Figure 1

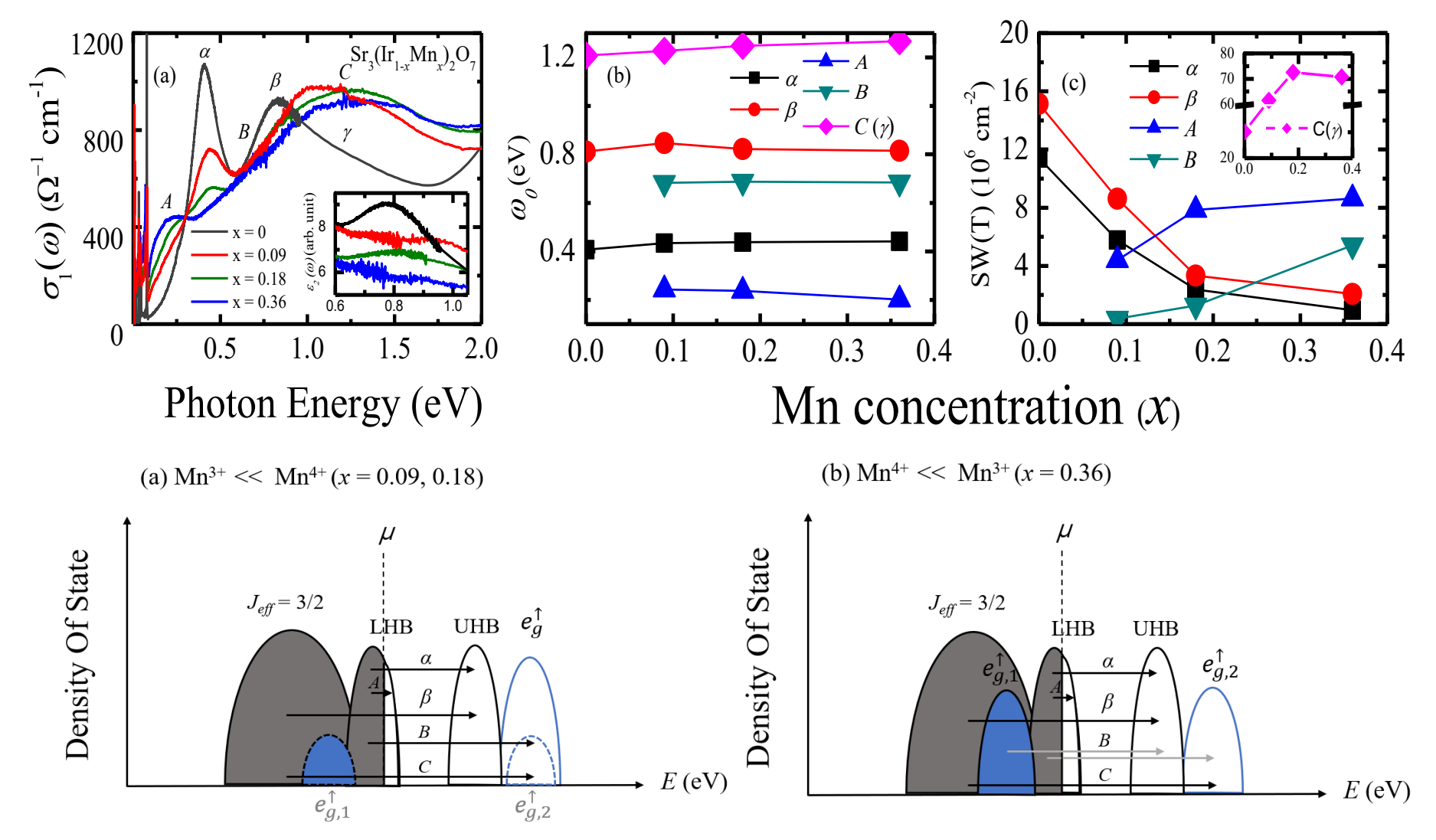


Figure 2

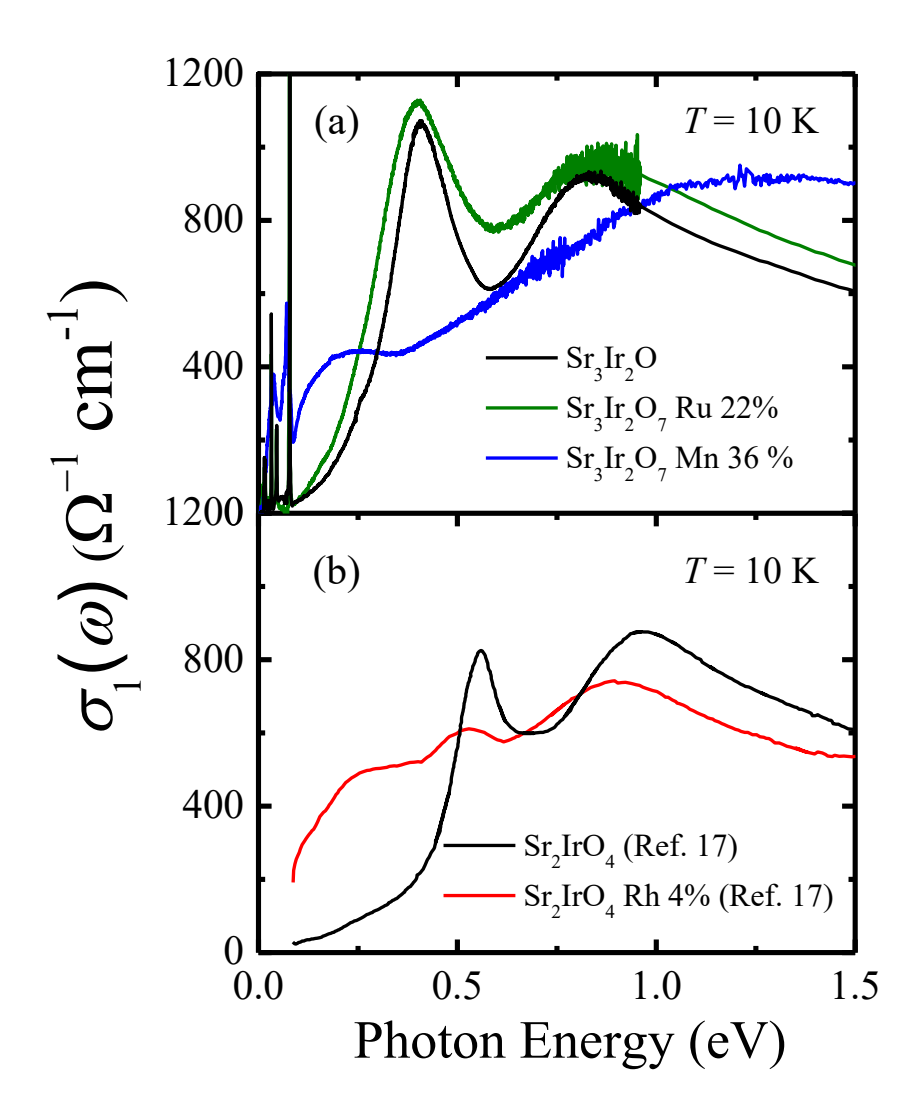


Figure 3

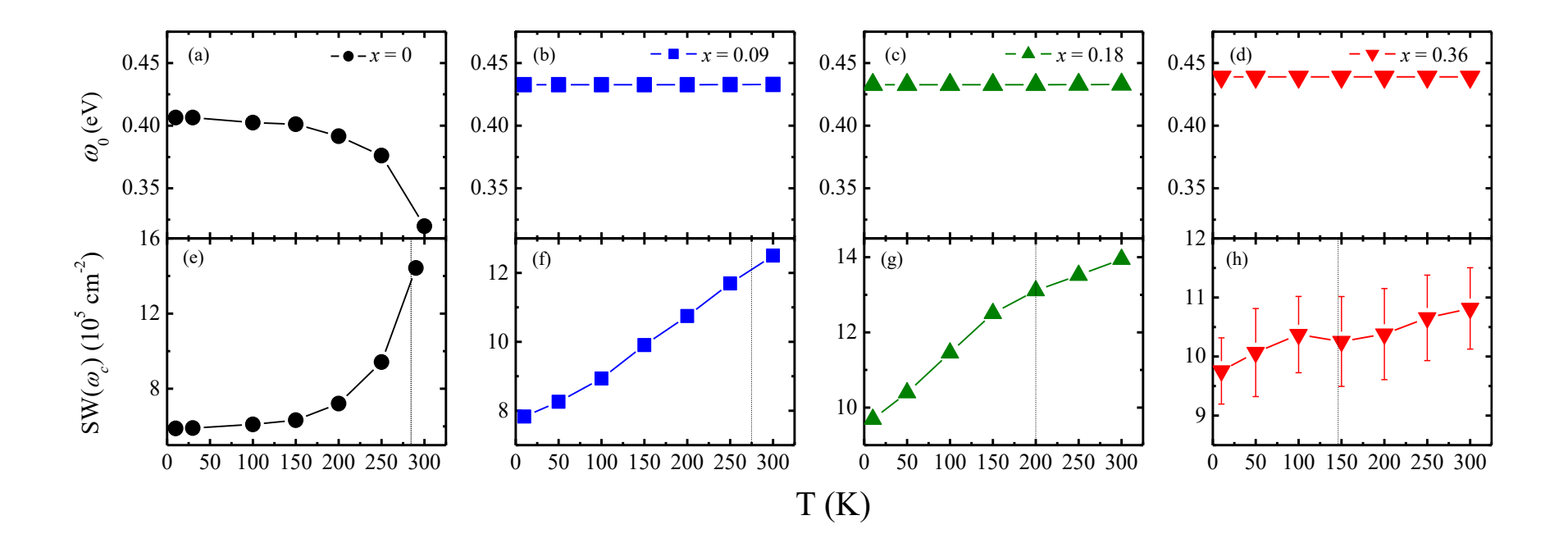


Figure 4